EARTH SURFACE PROCESSES AND LANDFORMS
*Earth Surf. Process. Landforms* (2019)

Published online in Wiley Online Library
(wileyonlinelibrary.com) DOI: 10.1002/esp.4564

# Ecohydrologic feedbacks controlling sizes of cypress wetlands in a patterned karst landscape

**Xiaoli Dong,[1,2]* A. Brad Murray[1] and James B. Heffernan[1]**
[1] Nicholas School of the Environment, Duke University, Durham, NC U.S., 27708
[2] Department of Environmental Science and Policy, University of California, Davis, CA US, 95616

Received 22 April 2018; Revised 22 November 2018; Accepted 3 December 2018

*Correspondence to: Xiaoli Dong, Department of Environmental Science and Policy, University of California, Davis, CA, U.S. 95616. E-mail: xldong@ucdavis.edu

ESPL
Earth Surface Processes and Landforms

ABSTRACT: Many landforms on Earth are profoundly influenced by biota. In particular, biota play a significant role in creating karst biogeomorphology, through biogenic $CO_2$ accelerating calcite weathering. In this study, we explore the ecohydrologic feedback mechanisms that have created isolated depressional wetlands on exposed limestone bedrock in South Florida – Big Cypress National Preserve –as a case study for karst biogeomorphic processes giving rise to regularly patterned landscapes. Specifically, we are interested in: (1) whether cypress depressions on the landscape have reached (or will reach) equilibrium size; (2) if so, what feedback mechanisms stabilize the size of depressions; and (3) what distal interactions among depressions give rise to the even distribution of depressions in the landscape. We hypothesize three feedback mechanisms controlling the evolution of depressions and build a numerical model to evaluate the relative importance of each mechanism. We show that a soil cover feedback (i.e. a smaller fraction of $CO_2$ reaches the bedrock surface for weathering as soil cover thickens) is the major feedback stabilizing depressions, followed by a biomass feedback (i.e. inhibited biomass growth with deepening standing water and extended inundation period as depressions expand in volume). Strong local positive feedback between the volume of depressions and rate of volume expansion and distal negative feedback between depressions competing for water likely lead to the regular patterning at the landscape scale. The individual depressions, however, are not yet in steady state but would be in ~0.2–0.4 million years. This represents the first study to demonstrate the decoupling of landscape-scale self-organization and the self-organization of its constituent agents. © 2018 John Wiley & Sons, Ltd.

KEYWORDS: biogeomorphology; chemical weathering; karst; landform evolution; self-organization

## Introduction

Biota and geomorphology interact to affect landscape form and evolution (Dietrich and Perron, 2006; Murray *et al.,* 2008). Vegetation controls or mediates weathering (Berner, 1992; Egli *et al.,* 2008), erosion (Toy *et al.,* 2002), and sediment transport (Istanbulluoglu and Bras, 2005; Corenblit *et al.,* 2009), and such influences are manifested in landscape morphology (Larsen and Harvey, 2010) and in the physical and ecological stability of ecosystems (Heffernan, 2008; Kirwan and Guntenspergen, 2010). Landforms in turn affect biota, and reflect the integrated influence of geology, climate, and time, as well as biota. While some landforms are created independent of significant direct biological influences, most landscapes on Earth are affected to various degrees directly by the biosphere, forming biogeomorphic landscapes (Stallins, 2006). Topography in such landscapes is closely and directly linked to biotic activity (Corenblit *et al.,* 2009), and the landforms are sometimes considered 'extended phenotypes' of biota (Phillips, 2016a).

Karst landscapes are a typical example of landforms resulting from reciprocal biotic–abiotic interactions (Phillips, 2016b). Slow dissolution of calcite can occur in water with $CO_2$ from the atmosphere being the only source of acidity. Biogenic $CO_2$ can accelerate chemical weathering by up to ~20 times (Dong *et al.,* 2018). Regardless of the source of acidity and the rate of weathering, cavities enlarge and coalesce and become hydraulically interconnected, forming sinkholes, conduits, and other preferential flowpaths that further entrain flow, creating a runaway positive feedback that expands features as long as drainage from weathering sites is relatively unrestricted (Sauro, 2012). This fundamental karstification feedback is reflected in the high connectivity and fractal shape of many subsurface karst features, whose sizes often follow power-law distributions (Maramathas and Boudouvis, 2006). However, many other karst features, including macro- and micro-topographic features, exhibit distinct topographic modes that are often arranged periodically or regularly in space. The presence of these distinct elevation modes and their distribution in space suggest the action of inhibitory feedbacks, locally and at a distance (Strudley *et al.,* 2006; Cohen *et al.,* 2011). Understanding the evolution of karst landscapes therefore requires that we consider additional feedback dynamics whose interactions are more complex than the well understood positive feedbacks between weathering rate and hydrologic conductivity.

The restriction of vertical drainage by low relief, subsurface aquicludes, or regional hydrologic base level is one potential constraint that would limit indefinite expansion of karst landforms. In landscapes where vertical drainage is restricted,

wetland plants often exploit depressions to form geographically isolated wetlands (Homoya and Hedge, 1982; Tihansky, 1999). Such depressions could continue to expand if surface flow or other hydrologic connection allows for continued export of dissolved calcite; however, if increased storage in the depression restricts the frequency and magnitude of surface water export, expansion would cease (Cohen *et al.,* 2011). Thus, when weathering products are primarily lost by surface drainage, increased storage and reduced runoff due to volume expansion is one potential negative feedback on depression growth. Differential evapotranspiration (ET) between depressions and their surroundings (higher ET in depressions) could exacerbate or even create this feedback (Eppinga *et al.,* 2009) if hydrologic losses from the depression are intensified and could also restrict depression growth by inducing inflow of minerals derived from upland weathering.

The accumulation of soil over limestone bedrock significantly alters the evolution of landscape topography. Accumulation of soil affects the residence time and flow of water in the soil, each of which have an important impact on chemical weathering. The rates of bedrock weathering are very slow in thick soils or in very thin soils, with maximum weathering at intermediate soil thickness (D'Odorico, 2000; Dong *et al.,* 2018). Such a hump-shaped relationship is shown in many studies to generate bistable geomorphic features (D'Odorico, 2000; Strudley *et al.,* 2006; Heffernan *et al.,* 2013). Another potential stabilizing feedback is the sensitivity of vegetation to hydrologic conditions. Plants that fuel dissolution require environmental conditions whose exceedance may cause mortality and reduce $CO_2$ production in soils, thereby reducing rates of weathering. Both soil thickness and plant hydrologic tolerances create potential negative feedbacks by reducing acidity available for weathering.

The expansion of depressions has the potential to influence weathering rates in adjacent areas through changes in hydrology, i.e. distal feedbacks. Scale-dependent feedbacks (SDF) – that is, local positive and distal negative feedbacks – are shown in landscapes around the world to generate strikingly regular patterns (Rietkerk and van de Koppel, 2008; Tarnita *et al.,* 2017). To generate regular rather than fractal spatial pattern, these feedbacks must operate at a distance, but not globally (i.e. they must have a particular length scale rather than a diffuse influence on all surroundings; Reitkerk and van de Koppel, 2008; Acharya *et al.,* 2015). While SDF-based models have been hugely successful in reproducing spatial arrangement of elements, the attributes of individual elements making up the spatial pattern are seldom taken into consideration. In a rare recent example, Tarnita *et al.* (2017) coupled colony behaviors of termites with SDF to reproduce both the characteristics of individual elements and the spatial arrangement of elements as a whole across the landscape, i.e. multiple simultaneous self-organizational processes. In general, however, it remains unclear whether the establishment of regular pattern implies or requires that individual patches (or landscape elements) are at equilibrium (defined in this study as the volume of depressions asymptotically approaching a steady state value) in terms of size.

In this paper, we explore the ecohydrologic feedbacks that have created isolated depressional wetlands on exposed limestone bedrock in South Florida – Big Cypress National Preserve – as a case study for karst biogeomorphic processes giving rise to regularly patterned landscapes. Big Cypress is located on a flat landscape, and features overdispersed (evenly spaced) limestone depressions (Watts *et al.,* 2014), made visually striking by the associated 'cypress domes' (cypress trees growing in a depression are taller nearer the center, forming a dome shape in the vegetation heights; Figure 1(D)). These depressions average 80–100 m in diameter, have bedrock elevations 1.5–2 m lower than the upland land surface, and cover ~25% of the landscape. Depressions have hydroperiods of ~300–350 days, and the surrounding matrix of pine and wet prairie upland mosaics (Figure 1; Watts *et al.,* 2014) are also inundated for ~50–150 days during most years. Recent studies have shown that weathering rates in Big Cypress are controlled

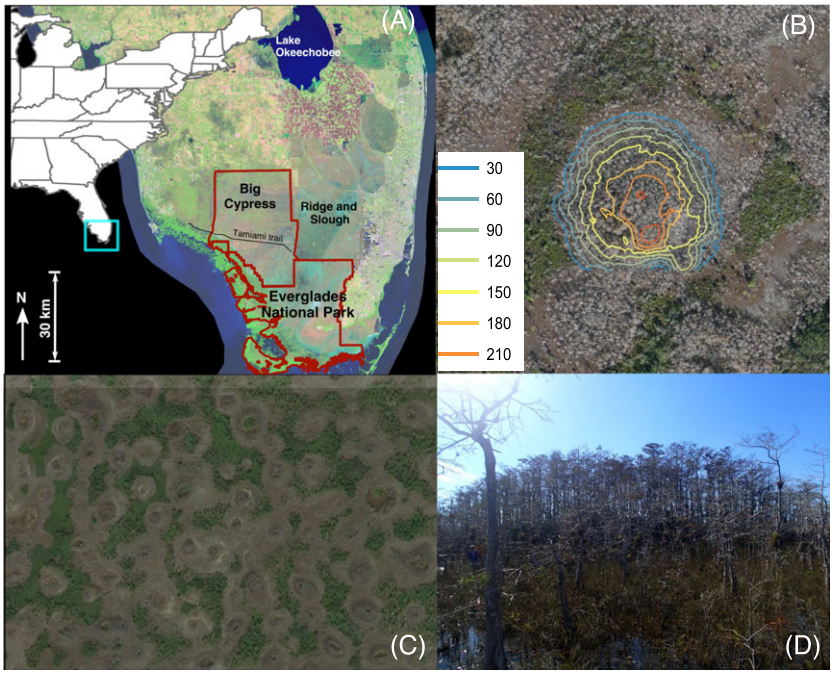


**Figure 1.** Map of Big Cypress National Preserve and the spatial pattern of cypress domes. (A) Big Cypress National Preserve is located in South Florida, bordering on the Everglades National Park; (B) contour map of soil thickness (cm) within a cypress depression; (C) regular-patterned cypress depressions on the landscape; and (D) Cypress domes: cypress trees in the center are taller than the cypress trees on the edge of the depression, forming a dome shape. [Colour figure can be viewed at wileyonlinelibrary.com]

by interactions between soil depth, climate, and biota (Dong *et al.,* 2018), and have used calcium and phosphorus mass-balance to evaluate theoretical estimates of depression age and weathering rate (Chamberlin *et al.,* 2018). Our objective for this study is to identify the mechanisms controlling the evolution of individual cypress depressions in Big Cypress and its relation with the patterned landscape as a whole.

A variety of positive feedbacks favor the differential weathering and expansion of domes relative to their surrounding uplands. Initial expansion of depressions increases hydrologic inflows by capturing additional runoff from surrounding uplands. This additional water input increases the potential for export of weathering products, reduces drought stress, and extends inundated periods that favor weathering by inhibiting $CO_2$ loss to the atmosphere (Dong *et al.,* 2018). Moreover, the expansion of depressions coincides with soil development, which favors higher biomass and organic matter accumulation. Because these positive feedbacks are presented and evaluated elsewhere (Dong *et al.,* 2018), we focus here on three hypotheses about local negative feedbacks that might constrain the weathering rate of large, established depressions:

- Hypothesis 1a. (Volume-export hypothesis of ET mechanism): increasing storage and evapotranspiration reduce surface and subsurface flow export, limiting depression expansion through reduced export of weathering products.
- Hypothesis 1b. (Mineral pump hypothesis of ET mechanism): differential evapotranspiration induces inflow of shallow groundwater carrying weathering products from the uplands, reducing net $Ca^{2+}$ export and limiting dome expansion.
- Hypothesis 2. (Soil cover hypothesis of soil thickness–transport mechanism): Thicker soil cover reduces weathering by limiting transport of $CO_2$ from the shallow root zone to the bedrock surface and of weathering products from bedrock surface to surface water.
- Hypothesis 3. (Biomass hypothesis): Increasing water depths and hydroperiods inhibit tree growth and recruitment, reducing $CO_2$ supply for weathering.

An equilibrium landscape occurs when one or all of these mechanisms reduce the rate of weathering in depressions to be equal to that in the upland matrix. We additionally predict that local positive feedbacks that favor depression expansion lead to an inevitable distal negative feedback: less water in the upland matrix, including nascent neighboring depressions imbedded in the upland matrix. This inhibition of upland weathering, if operating over limited spatial scales, resulting in scale-dependent feedback, could contribute to the formation of regular patterning in the landscape (Rietkerk and van de Koppel, 2008). In this paper, we build a numerical model to simulate the growth of individual cypress depressions and to evaluate the roles of the hypotheses described above.

# Methods

## Site description

Big Cypress National Preserve is located in southwest Florida, USA. It is a low relief landscape of ~3000 $km^2$ in area with limestone bedrock exposed or near the land surface (Figure 1). Because the geologic formations under Big Cypress are slightly mounded in relation to the surrounding landscapes, Big Cypress is entirely rain-fed, with hydrology driven strongly by precipitation regime. Low relief (~5 cm $km^{-1}$) and high annual precipitation (150 cm $yr^{-1}$) lead to prolonged periods of slow-moving sheet flow. In cypress depressions, the annual inundation period can last > 300 days, punctuated by periods with no surface water (Watts *et al.,* 2012).

Cypress trees (*Taxodium distichum*) form dome shapes with trees on the edge of the dome shorter and those in the center taller (Figure 1(D)). Underneath cypress trees are wetland depressions created by chemical weathering of limestone bedrock. Currently, depressions are 30–50 m in radius and 1.5–2 m deep in the center. The area of wetland depressions occupies about 24% of the entire landscape. Bedrock in depressions is covered by a thick layer of sediment and fine soils (Figure 1(B)) generated by regolith from insoluble weathering minerals and organic matter accumulation. The ratio of thickness of soil cover to bedrock depth is ~0.6 (Watts *et al.,* 2014). $CO_2$ generated by biological respiration (root respiration and decomposition of organic matter) augments chemical weathering by ~ 20 times (Dong *et al.,* 2018). Cypress depressions are evenly spaced in an upland matrix consisting of pine trees (*Pinus elliottii*), marl prairie (dominated by *Muhlenhergia capillaris*), and cypress prairie (*Taxodim distichum*). Several lines of evidence support the inference that depressions started to develop in the early Holocene (Chamberlin *et al.,* 2018; Dong *et al.,* 2018).

## Hydrological processes

Our model simulates the expansion of an individual cypress depression in volume over time via chemical weathering of bedrock. Each cypress depression is associated with its hexagonal upland catchment (average number of nearest neighbor = 6; data not published), with its edge length of 100 m (i.e. radius of catchment). This value is chosen based on an average distance between the centers of two nearest cypress depressions of ~200 m (Watts *et al.,* 2014).

We model weathering rates in both depressional areas and in the upland catchment as a function of soil depth, hydrologic conditions, and biotic activities, using rules derived from the vertical reaction-transport model of Dong *et al.* (2018). This mechanistic model successfully predicts vertical distribution of dissolved $Ca^{2+}$ and $CO_2$ in inundated soils of Big Cypress, and generates estimates of depression age that closely align with empirical estimates based on both mass-balance estimates of weathering and radio-carbon dating (Chamberlin *et al.,* 2018). Weathering rate is sensitive to the hydrological state of soil cover on bedrock. The model includes five hydrological processes (at daily time scale) to describe the hydrological dynamics in cypress depressions and their associated upland catchments. These processes are: precipitation, surface flow drainage ($v_s$), evapotranspiration (ET), regional groundwater drainage (*GW*), and local subsurface exchange ($v_{sub}$; Figure 2). Wetland stage is described with the daily water balance equation:

$$y_{w,t+1} = y_{w,t} + \frac{dy_w}{dt} \tag{1}$$

$$\frac{dy_w}{dt} = \begin{cases} \frac{1}{S_{soil}}(P - V_{sub\_w} - rET_w - GW), & y_w < Z_w + z_s \\ P - V_{sub\_w} - rET_w - GW, & Z_{up} \geq y_w \geq Z_w + z_s \\ P - V_{sub\_w} - rET_w - GW - \frac{4v_s}{3}Slp, & y_w > Z_{up} \end{cases} \tag{2}$$

where $S_{soil}$ is specific yield of soils in cypress depressions. $Z_w$ and $z_s$ are the elevation of bedrock in depressions and the thickness of soil cover; hence, $Z_w + z_s$ represents the elevation of the

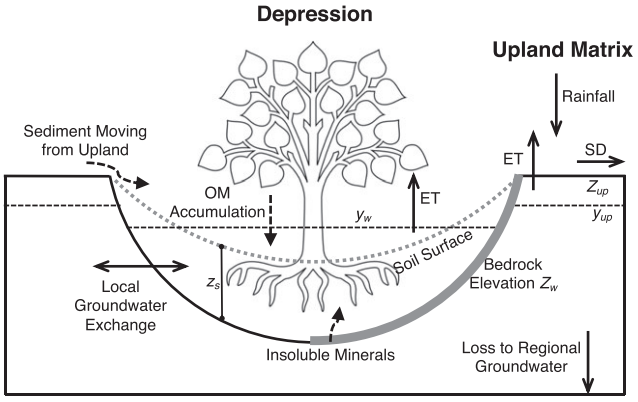


**Figure 2.** Schematic of hydrological and soil processes in the numerical model of cypress depressions. Solid arrows indicate hydrological processes in the model: precipitation, evapotranspiration (ET), local groundwater exchange between basin and upland matrix, recharge to regional groundwater, and surface drainage (SD). Dashed arrows represent processes contributing to soil accumulation inside the depression: sediment moving from upland, organic matter (OM) accumulation, and accumulation of insoluble minerals from limestone weathering. The model simulates these processes at each grid along the generatrix of the depression (the thick gray line).

soil surface in depressions. $Z_{up}$ is the upland bedrock elevation. Similarly, upland water table elevation is simulated as:

$$y_{u,t+1} = y_{u,t} + \frac{dy_u}{dt} \tag{3}$$

$$\frac{dy_u}{dt} = \begin{cases} \frac{1}{S_b}\left(P + V_{sub\_up} - rET_u - GW\right), & y_u < Z_{up} \\ P + V_{sub\_up} - rET_u - GW - \frac{4v_s}{3}Slp, & y_u \geq Z_{up} \end{cases} \tag{4}$$

where $S_b$ is the specific yield of limestone bedrock. The time step of changes in water table is day, that is, $\Delta t = 1$. This term is omitted in Equations (1) and (3).

Following Rodriguez-Iturbe *et al.* (1999), daily rainfall (mm $d^{-1}$) is modeled as a Poisson process P ($\lambda_P$, $\alpha$) with exponentially distributed rainfall depths (mean = $\alpha$) and frequency $\lambda_P$ (mean number of days between rainfall events = $1/\lambda_P$). Rainfall frequency and depth were parameterized ($\lambda_P = 0.37$ and $\alpha = 9.9$ mm) with 2002–2017 precipitation data for South Florida (USGS Everglades Depth Estimation Network; https://sofia.usgs.gov/eden/eve/index.php?rainfall=rainfall), yielding a mean annual precipitation of 1337 mm. We assume no significant change in annual precipitation (climate) over time.

Daily regional groundwater drainage (*GW*) is slow, and we prescribe a constant rate of 0.55 mm $day^{-1}$ (i.e. 0.2 m $yr^{-1}$) (McLaughlin *et al.*, 2014). The rate of local subsurface exchange ($m^3$ $d^{-1}$) between upland matrix and the depression is determined by head gradients (d*h*) between upland water table and wetland stage, a flow length (d*l*) equal to the distance between upland centroid and wetland stage, saturated hydraulic conductivity ($K_{sat}$), and the cross-sectional area for exchange ($A_x$) (Figure 2):

$$v_{sub} = (A_x K_{sat})\frac{\partial h}{\partial l} \tag{5}$$

$v_{sub}$ ($m^3$ $d^{-1}$) is converted to the amount of water table drop in a day in the upland $V_{sub\_up}$ and in the depression $V_{sub\_w}$ (this is realized numerically, as the model tracks the temporal evolution of shape of the depression, a volume of $v_{sub}$ water can be translated to corresponding increase/decrease of water table in the upland and in the depression in the given time step).

We used Manning's equation to estimate the rate of surface sheet flow ($v_s$). Manning's equation, derived empirically for turbulent flow in unvegetated channels, accounts only for frictional resistance arising from drag exerted by the channel bottom. Water moving in wetland systems, such as Big Cypress, on the other hand, is characterized by laminar flow regimes, and frictional resistance arises predominantly from drag by emergent vegetation throughout the water column. We follow the formulation by Kadlec (1990) to describe rate of surface flow in vegetated environments (m $d^{-1}$):

$$v_s = \begin{cases} K_f d^{\beta} S_f^{\lambda}, & y_{up} > Z_{up} \\ 0, & y_{up} \leq Z_{up} \end{cases} \tag{6}$$

where $S_f$ is the friction slope in $x$ direction, $d$ is water depth (m), $K_f$ is the surface-water conductivity coefficient ($m^{(1-\beta)}$ $day^{-1}$), and $\beta$ and $\lambda$ are exponents. Values of $K_f$, $\beta$, and $\lambda$ are usually determined through calibration. $\beta$ depends on micro-topography as well as vegetation stem density distribution and a value of 3.0 is used in this study for the vegetated bed (Kadlec, 1990). $\lambda$ depends on flow regime, ranging between 0.5 and 1 (Kadlec and Knight, 1996). We used $\lambda = 0.8$ following Bolster and Saiers (2002), who modeled surface hydrology regime in a similar system in South Florida. We used $K_f = 3.8\times10^7$, a lower value within the normal range of $K_f$ (Kadlec, 1990). For wetland environments, with gentle ground-surface slopes, the acceleration terms in the momentum equations can be neglected (Bolster and Saiers, 2002). Gravitational forces balance frictional forces and the friction slope can be expressed as:

$$S_f = -\frac{\partial H}{\partial s} \tag{7}$$

where $H$ is the hydraulic head ($H = z + d$, where $z$ is the bedrock elevation of the upland matrix and $d$ is the water depth; m), and $s$ is distance in the downstream direction. When water depth varies between 0.1 and 0.5 m, with the parameter values we chose above, $v_s$ varies between 0.6 and 71.2 m $day^{-1}$, a range that captures a realistic flow regime in Big Cypress. *Slp* is the mean landscape relief (5 cm $km^{-1}$). $2\sqrt{3}R^2 v_s \times Slp$ ($m^3$ $d^{-1}$) describes the amount of water lost from the catchment (depression area included) via surface drainage in a day. Therefore, rate of drop in surface water table ($V_{s\_v}$; m $d^{-1}$) caused by surface drainage is $\left(2\sqrt{3}R^2 v_s \times Slp\right)/\left(1.5\sqrt{3}R^2\right) = {}^4/_3 v_s Slp$.

ET occurs both in cypress depressions and in the upland matrix. Daily ET rate in depression patches ($rET_w$) and in pine tree upland patch ($rET_u$) are modeled as an exponential decline from potential ET (*PET*) (Laio *et al.*, 2009), assuming an exponential distribution of root biomass (Schenk and Jackson, 2002):

$$rET_w = PET_w \times e^{-(Z_w + z_s - y_w)/RD_c} \tag{8}$$

$$rET_u = PET_u \times e^{-(Z_{up} - y_{up})/RD_p} \tag{9}$$

$$PET_w = \kappa PET_{up} \tag{10}$$

where $(Z_w + z_s - y_w)$ and $(Z_{up} - y_{up})$ describe the distance from water table to surface in cypress depressions and in the upland matrix, respectively. $RD_c$ and $RD_p$ are the rooting depth of cypress trees (m) in depressions and pine trees on the upland matrix. We use the soil depth above which 90% of root biomass grows for the parameter values of $RD_c$ and $RD_p$. For $RD_p$, we use a constant of 0.3 m, which is representative of

pine tree uplands in the coastal plain of South Florida (Van Rees and Comerford, 1986). To calculate $RD_c$, the vertical distribution of root biomass density is simulated following Dong *et al.* (2018):

$$B_r = A\left(\frac{blm}{e^{Az_s}}\right)e^{Az} \tag{11}$$

where *blm* is belowground biomass (kg m$^{-2}$; it is calculated from soil thickness as described in Appendix A), $z_s$ is soil thickness at a given location in a depression (cm), and $z$ is the distance to soil–bedrock interface (cm). Parameter $A$ controls the vertical distribution of root biomass, and for Big Cypress, a value of 0.02 is used (Dong *et al.*, 2018). $PET_{up}$ is potential ET in the upland matrix, and is set at a constant of 0.9 m yr$^{-1}$ (Shoemaker *et al.*, 2011), assuming no significant change of upland biomass over time. We set $PET_w$ to be $\kappa$ times $PET_{up}$. $\kappa$ is determined by the biomass in cypress depressions. In the contemporary landscape, $\kappa$ is ~120% (Shoemaker *et al.*, 2011). $\kappa(t)$ is therefore estimated by 1.2 multiplied by the ratio between geometric mean of aboveground biomass (represented by tree height) over an entire depression in the year $t$ to geometric mean of aboveground biomass across a representative depression (radius = 50 m, depth in the center = 2 m, with soil thickness taking up 60% bedrock depth) in the contemporary time.

## Biological processes and $CO_2$ production

Biological respiration provides an important $CO_2$ subsidy for chemical weathering. We consider two variables influencing root biomass: (1) inundation-period (Megonigal and Day, 1992); and (2) water depth (Harms *et al.*, 1980). Following Dong *et al.* (2018), we did not explicitly model recruitment, growth, and mortality of trees; instead, total respirational $CO_2$ produced in soil is correlated to the aboveground biomass, which is a function of tree height. Tree height is estimated from thickness of soil cover with a logistic function parameterized by empirical data collected in Big Cypress (Appendix A):

$$H_{tr} = \frac{H_{max}}{1 + e^{-b(z_s - a)}} \tag{12}$$

where $z_s$ is the thickness of soil cover. $a$ and $b$ are parameterized by empirical data (Appendix A). $H_{max}$ is the maximum height of a cypress tree in the general case ($H_{max}$ = 30 m).

Mortality of cypress is closely related to maximum water depth during inundation. Harms *et al.* (1980) found that mortality of cypress trees progressively increases as prevailing water depth exceeds 1.3 m. We construct a piecewise function to describe the detrimental effect of maximum water depth during inundation period on root biomass, parameterized by the empirical tree mortality and water depth relationship by Harms *et al.* (1980):

$$\gamma_1 = \begin{cases} \max(0, -0.025 + 0.15 \times WD_{90}), & WD_{90} < 1.3 \\ \min\left(1, \dfrac{0.17}{e^{(0.17 - WD_{90})}}\right), & WD_{90} \geq 1.3 \end{cases} \tag{13}$$

$WD_{90}$ (m) refers to the maximum water depth that lasts at least 90 days in a year.

Inundation duration further influences root growth (therefore, influences $CO_2$ production). Continuously flooded cypress trees have low root-to-shoot ratios (Megonigal and Day, 1992) and shallow root systems and a hump-shaped relationship between root production and hydroperiod is established for cypress trees (a too short and a too long flooding period both inhibit growth) (Mitsch and Ewel, 1979; Day and Megonigal, 1993). Based on these empirical studies, we prescribe a hump-shaped function to describe the modification of hydroperiod on root biomass:

$$\gamma_2 = \frac{1}{e^{\left(\frac{0.75T_{in} - 183}{150}\right)^2}} \tag{14}$$

where $T_{in}$ (day) is the number of days of inundation in a year. This gives a maximum growth ($\gamma_2 > 0.9$) when the inundation period is between 180 and 300 days in a year.

The actual tree height $H_{tr}$ is therefore modified by these two hydrologic factors as $H_{tr} \times (1 - \gamma_1) \times \gamma_2$. $CO_2$ production ($P_{CO2}$, g C m$^{-2}$ yr$^{-1}$) is indirectly derived from tree height as detailed in Dong *et al.* (2018) (and also in Appendix A).

## Soil accumulation

Four processes contribute to soil accumulation in cypress depressions: (1) accumulation of insoluble minerals from weathered bedrock, $R_{dis}$; (2) organic matter accrual ($R_{OC}$; e.g. leaf fall, roots); (3) organic matter loss in peat fires, $R_{fire}$; and (4) sediments moving from upland into the depression, $q_{up}$. Daily soil elevation change (m day$^{-1}$) is described as:

$$\frac{\partial(z_s + Z_w)}{\partial t} = -K\frac{\partial^2(z_s + Z_w)}{\partial x^2} + \frac{R_{dis} + R_{OC} + R_{fire}}{365} \tag{15}$$

where $z_s$ is the thickness of soil cover and $Z_w$ is the bedrock elevation in a depression. Soil movement is simulated through an analogy with Fick's law of diffusion. Along the slope inside a depression, soil flux $q_s$ is proportional to the soil elevation gradient $\nabla(z_s + Z_w)$:

$$q_s = K\nabla(z_s + Z_w) \tag{16}$$

$K$ is linear diffusivity in soil creep, and we use a value of $2 \times 10^{-4}$ m$^2$ yr$^{-1}$ (Martin and Church, 1997; Roering *et al.*, 1999). $R_{dis}$ is the rate of accumulation of insoluble minerals (m yr$^{-1}$). In Big Cypress, limestone contains ~10% insoluble minerals. Therefore,

$$R_{dis} = \frac{dZ_w}{dt} \times 10\% \tag{17}$$

$R_{OC}$ is the rate of organic matter accrual in depressions (m yr$^{-1}$) and is described as:

$$R_{OC} = \frac{P_{OC}}{\rho_{OC}} \tag{18}$$

where $P_{OC}$ is the annual organic matter production (kg m$^{-2}$ yr$^{-1}$), and $\rho_{oc}$ is the density of organic matter (kg m$^{-3}$). Under the current vegetation and hydrologic state, organic matter accretion rate in the region is about 0.27–1.13 cm yr$^{-1}$ (Reddy *et al.*, 1993). We assume that the current accretion rate of organic matter is correlated to current belowground biomass (estimated from soil thickness in Appendix A). We apply the same relationship over the course of depression evolution to estimate $P_{OC}$.

$R_{fire}$ is the rate of reduction of organic matter by peat fires (m yr$^{-1}$). In South Florida, cypress swamps have long hydroperiods that promote development of organic soils, but occasionally experience severe droughts that expose them to the occurrence of ground fire as frequently as every 100–150 years (Snyder, 1991). The combustion of soil organic matter lowers

soil elevations. Soil organic carbon combusted in one fire event averages about 4.18 kg m$^{-2}$, about 1–5% of the organic matter cover (Watts, 2013). In the model, we assume that during each peat fire event (occurring every ~150 years), 3% of the existing organic matter is lost.

Sediments moving from upland matrix to depression occurs by entering from the edge of a depression. Therefore, $q_s$ is a boundary condition (positive direction: from edge of the depression to the center; m$^2$ day$^{-1}$). $q_s$ is limited by total amount of sediments available on the upland (assuming zero sediment in the initial condition, and all the sediments in the upland are from insoluble minerals from upland weathering). The boundary on the edge of a depression is expressed as:

$$q_s(0,t) = \begin{cases} K\dfrac{(z_s(0,t)+Z_w(0,t))-Z_{up}}{\Delta z}, & 2\,\pi r(t) q_s \Delta t \le V_{s_{up}} \\ \dfrac{V_{s_{up}}}{2\,\pi r(t)\,\Delta t}, & 2\,\pi r(t) q_s\,\Delta t > V_{s_{up}} \end{cases} \tag{19}$$

where $V_{s_{up}}(t)$ (m$^3$) is the total amount of sediments available on the upland matrix at time $t$. It is calculated assuming the remaining insoluble minerals (in Big Cypress, ~10% of limestone) from upland bedrock weathering are the sole influx, and flux into depressions is the only export. $r(t)$ is the radius of the depression at time $t$. In the very center of a depression, we assume it is flat, and the boundary condition is zero flux:

$$q_s(L,t) = 0 \tag{20}$$

## Bedrock weathering

Bedrock weathering occurs in both the upland and in depressions (Figure 2). The rate of chemical weathering is limited by $CO_2$ available at bedrock surface and the export of weathering products out of depressions. $CO_2$ generated by biological respiration is the major source of acidity for chemical weathering in Big Cypress (Dong *et al.,* 2018). $CO_2$ available at bedrock surface is ultimately limited by two processes: the total amount of $CO_2$ generated by biological respiration in the root zone and the transport of $CO_2$ to bedrock surface from root zone (another part of $CO_2$ is transported upwards and is lost to the atmosphere). Weathering products can be exported from the bedrock surface via the lower boundary (to groundwater) and via the upper boundary (to surface flow).

Of the $CO_2$ generated by biological respiration, only a fraction is transported to the bedrock surface for chemical weathering, and this fraction decreases as soil cover on bedrock thickens. Hydrological state of soils and the thickness of soil cover on bedrock are the two key variables determining $CO_2$ retention (defined as the ratio of $CO_2$ reaching bedrock surface for weathering to total amount of $CO_2$ produced in unit time) (Dong *et al.,* 2018). Specific to conditions in Big Cypress, a function describing $CO_2$ retention ($RET_{CO2}$) is extracted from results of a limestone weathering model developed by Dong *et al.* (2018) for Big Cypress as follows (Figure S1, Supplementary information):

$$RET_{CO2} = \begin{cases} \dfrac{1.05}{e^{1.5\times(z_s+0.7)}}, & y_w \ge z_s + Z_w \\ \dfrac{0.88}{e^{2.6\times(z_s+0.7)}}, & y_w < z_s + Z_w \end{cases} \tag{21}$$

When the rate of chemical weathering is export limited (i.e. the amount of $Ca^{2+}$ released by $CO_2$ in a year > the amount of $Ca^{2+}$ that can be exported via groundwater and via surface flow), the total amount of calcite weathered in a year of an entire depression equals the capacity of the landscape to export $Ca^{2+}$. $\vartheta$ is the position along the generatrix (total length = $L$) of a depression (thick gray line in Figure 2). Rate of mean annual weathering (m yr$^{-1}$) at location $\vartheta$ is described by:

$$\frac{dZ_w(\vartheta)}{dt} = \min\left(1, \frac{\frac{EXPT_{Ca}(t)}{\frac{M_{Ca}}{M_{CaCO_3}}}}{\sum_{\tau=1}^{365}\left(\int_{\vartheta=0}^{L}\left(2\pi\frac{P_{CO2}(\vartheta,\tau)\times RET_{CO2}(\vartheta,\tau)}{\frac{M_{CO_2}}{M_{CaCO_3}}}\,d\vartheta\right)\right)}\right) \times\left(\sum_{\tau=1}^{365}\frac{P_{CO2}(\vartheta,\tau)\times RET_{CO2}(\vartheta,\tau)}{\rho\frac{M_{CO_2}}{M_{CaCO_3}}}\right) \tag{22}$$

where $P_{CO2}$ is the amount of $CO_2$ produced (kg $CO_2$ day$^{-1}$ m$^{-2}$), $\rho$ is the density of limestone bedrock (kg m$^{-3}$), and $M_{CO2}$, $M_{Ca}$, and $M_{CaCO3}$ are the molecular weight per mole $CO_2$, per mole calcium, and per mole calcite (g mol$^{-1}$), respectively. The unit of $t$ is year, and $\tau$ is days in a year. $EXPT_{Ca}$ (kg $Ca^{2+}$ yr$^{-1}$) is the annual capacity of an entire depression to export $Ca^{2+}$:

$$EXPT_{Ca,t} = \sum_{\tau=1}^{365}\left(c\left[Ca^{2+}\right]_{w_{upper}}\times Q_{s,\tau} + c\left[Ca^{2+}\right]_{w_{lower}}\times Q_{gw,\tau}\right) \tag{23}$$

where $c[Ca^{2+}]_{w\_upper}\times Q_{s,\,t}$ described the total amount of $Ca^{2+}$ moving out of a depression via surface drainage in a given day. Similarly, $c[Ca^{2+}]_{w\_lower}\times Q_{gw,\,t}$ describes the total amount of $Ca^{2+}$ leaving a cypress depression via the lower boundary in a day. $Q_{s,t}$ is daily surface discharge (m$^3$ d$^{-1}$) and it is calculated by rate of surface water table drop ($V_{s\_v}$) multiplied by the area of a catchment (depression area included). $Q_{gw,t}$ is daily groundwater discharge (m$^3$ d$^{-1}$), calculated by groundwater discharge rate multiplied by the surface area of a depression below water table.

For chemical weathering in the upland matrix, we assume that subsurface water and surface flow moving out of the depression area is already saturated by dissolved calcium, without capacity for further weathering. The total weathering capacity of the upland is provided by dissolved $CO_2$ in rainfall in equilibrium with atmospheric $CO_2$. Change of upland bedrock elevation $Z_{up,t}$ (m yr$^{-1}$) is described by:

$$Z_{up,t} = Z_{up,t-1} + \frac{dZ_{up}}{dt} \tag{24}$$

$$\frac{dZ_{up}}{dt} = \sum_{\tau=1}^{365}\frac{Q_{up,\tau}[Ca]_{sat}}{\frac{M_{Ca}}{M_{CaCO_3}}\rho S_{up}} \tag{25}$$

where $[Ca]_{sat}$ is the saturated concentration of dissolved calcium in solution in equilibrium with atmospheric $CO_2$ pressure, i.e. $[Ca]_{sat}$ = 18.8 g m$^{-3}$, $Q_{up}$ is the amount of precipitation (m d$^{-1}$) that falls on the upland matrix after losses by surface runoff to depressions, and $S_{up}$ is the total area of the upland matrix. If precipitation generates overland flow after filling up the porous zone in the upland limestone, the overland flow does not contribute to the weathering capacity of the upland, but to the weathering of depressions. We assume surface runoff to depression is rapid, providing no time for upland weathering. In this case, $Q_{up}$ equals the volume of the porous zone in the upland before precipitation occurs multiplied by time $t$ (1 day). However, if precipitation is not sufficient to fill the upland porous zone, all precipitation contributes to $Q_{up,t}$ (that is, $Q_{up,t} = P$ x $S_{up}$ with no surface runoff to depressions).

The uncertainty associated with estimating export capacity is the calcium concentration in surface flow and in flow leaving

the system via groundwater (i.e. $c\ [Ca^{2+}]_{w\_upper}$ and $c\ [Ca^{2+}]_{w\_lower}$ in Equation (22)). Currently, calcium concentration within cypress depressions ranges between 29 and 109 mg $L^{-1}$ across the landscape ($n$ = 23), with mean = 56 mg $L^{-1}$ (standard deviation = 16.7). Calcium concentration in the pore water at or near bedrock surface in depressions ranges between 52 and 288 mg $L^{-1}$ ($n$ = 24), with mean of 158 mg $L^{-1}$ (standard deviation = 66.7). Over the course of the evolution of a cypress depression, we assume a linear relationship between calcium concentrations and the volume of biomass in the system. In the initial condition, biomass is zero and calcium concentration in exporting flows is in equilibrium with atmospheric $CO_2$ pressure; and with current biomass, calcium concentration in surface flow moving out of a depression is 56 mg $L^{-1}$ and in groundwater is 158 mg $L^{-1}$. We evaluated the model sensitivity to the slope of this linear relationship (the concentration of calcium in flows exporting via surface drainage and via groundwater drainage). Choice of slope alters the duration of the episode of export limitation, but does not change the general pattern of dominance by reaction limitation overall (Figure S2).

## Model analysis

### Analysis of steady state

We analyzed the steady state of basin expansions by monitoring the growth of a depression over time and calculating its expansion rate in radius, depth, and volume. The steady state is reached, when the expansion rate reaches zero asymptotically (when the volume expansion rate is $<10^{-4}$% every year). In practice, it is realized through the balance between reduction of the volume of depressions by upland weathering and increase of the volume of depressions by weathering inside depressions (Figure S3).

### Analysis of feedbacks

We assessed the relative strength of three feedback mechanisms by turning on or off the corresponding feedback, and running the model until the depression reaches steady state asymptotically. To eliminate the (1) *ET feedback,* we replace Equation (4) with $rET_w = rET_{up}$, which eliminates the ET differential between the uplands and the matrix. To eliminate the (2) *soil cover feedback,* we set $CO_2$ retention within the soil profile at a constant that equals the value at the initial condition, so that increasing thickness of soil cover has no effect on $CO_2$ delivery to the weathering front. We turn off the (3) *biomass feedback* by describing biomass only as a function of soil depth, eliminating the inhibition of vegetation by inundation period and maximum water depth during inundation. The effect of each feedback is analyzed by comparing the scenario of feedback off with the 'realistic' scenario, i.e. the scenario with all feedback mechanisms turned on.

### Model execution

In forming limestone depressions, coalescence of neighboring depressions is a common phenomenon (Fookes and Hawkins, 1988; Waele *et al.,* 2009). We expect such a process to occur also in Big Cypress. The model however does not explicitly simulate the process of basin coalescing or the associated morphometric fusion. Instead, we represent the depression coalescence by using different radius values in the initial condition. We run nine different simulations, corresponding to nine initial values for radius of a depression: 0.2 m, 1 m, 2.5 m, 5 m, 10 m, 20 m, 30 m, 40 m, and 50 m. Each model run contains one depression and its associated catchment (assigned at $R$ = 100 m), and if expansion of the depression reaches the edge of the catchment, the model is terminated (this did not happen when a realistic set of parameter values was used). In the model, the flat horizontal surface surrounding the depression is defined as 'upland (matrix)' and the surface that deviates below the upland makes up a 'depression' (Figure 2; Figure S3). The initial depth of a depression is set at 0.1 m. The initial soil cover is zero on the upland catchment. Inside the limestone pit, it is 30% of the bedrock depth (depth relative to upland elevation). We explore three scenarios of interest: (1) precipitation regime (+/- 20% of current annual precipitation); (2) the radius of upland catchment (increase to 150 m and decrease to 80 m from the default 100 m); and (3) rates of groundwater drainage (increase to 0.6 m $yr^{-1}$ and decrease to 0 from the default 0.2 m $yr^{-1}$).

# Results

## Geomorphic evolution of cypress depressions

According to model results, cypress depressions will continue to grow in both radius and depth over time, to sizes much greater than are found in the contemporary landscape (Figure 3).

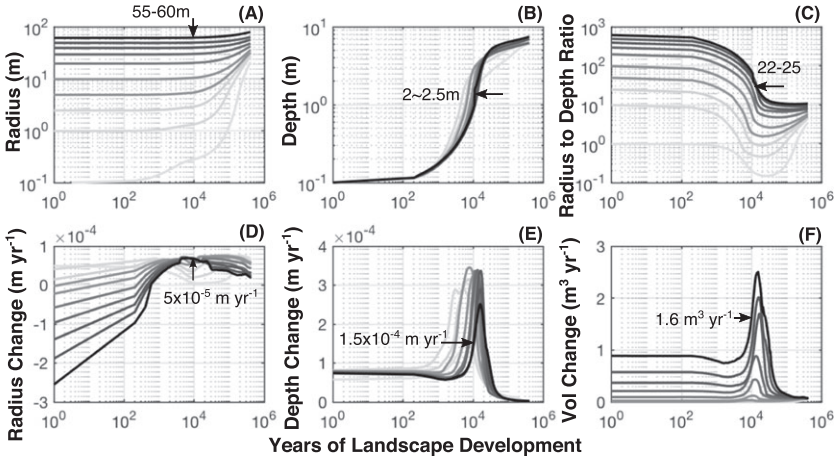


**Figure 3.** Change in the size of a cypress depression over time. Different lines in each plot represent different values of radius in the model initial condition: from lighter gray to darker gray with initial radius of 0.2 m, 1 m, 2.5 m, 5 m, 10 m, 20 m, 30 m, 40 m, 50 m, and 100 m (same initial depth = 0.1 m). (A-C) Changes of basin radius, depth (center of a depression), and radio-to-depth ratio over time (0.4 million years). (D-F) Changes of rate of radius expansion, of depth increase, and of volume expansion over time. Arrow in each plot indicated the value after 10,000 years of landscape development (approximately the condition of the present day).

Over time, the area of cypress depressions will become ~60% of the entire landscape as the landscape approaches an equilibrium state (when radius, depth, and volume no longer change or change at a negligible rate under current climate conditions). The size of depressions will eventually stabilize (Figure 3). The system reaches equilibrium state after about 0.2–0.4 million years from initiation, when the radius approaches 80 m and the bedrock depth in the depression center approaches 7.5 m (Figure 3(A)–(B)). Under the current precipitation regime and with depressions at their eventual steady state dimensions, the number of days when the whole landscape is inundated by overland flow will be reduced to ~80 days in a year.

The model results are not consistent with the hypothesis that each cypress basin in Big Cypress is grown entirely from one small dissolution pit. Without expansion of basin radius by coalescence of multiple small depressions, the radius would only have reached the order of meters (or less) since initiation of the landscape in the early Holocene (Figure 3(A)), while currently the radius of cypress depressions in Big Cypress is about 50–70 m. The expansion in the radius of depression continues to decline over time and drops to ~3.2 cm $kyr^{-1}$ in 0.2 million from present, i.e. an increase in the radius by $4.0\times10^{-5}$% per year. Vertical expansion of depressions at first increases (from 7.5 to 45 cm $kyr^{-1}$) as basins increase in volume, and then slows (to 0.24 cm $kyr^{-1}$, a relative increase of $3.2\times10^{-5}$% per year) (Figure 3(E); Figure 4 (C)). The maximum rate of depth increase occurs around 15 000 yr from the start of landscape development – that is about 6 kyr from present (Figure 3(E)). The equilibrium depth is about 7.5 m in the center of a depression, which will be reached in about 0.4 million years from today (currently 1.5–2 m deep, and it will be 6 m deep in ~0.1 million years from present) (Figure 3(A)–(B)). The decline in the expansion rate over time in vertical dimension is much more drastic (three orders of magnitude; Figure 3(E)) than the decline in lateral dimension (one order of magnitude; Figure 3(D)).

## Feedbacks

The rate of volume expansion first increases as the volume of a depression increases, and then decreases (Figure 4(A)), indicating a shift in the relative importance of positive feedbacks in small depressions and negative feedbacks for larger depressions. After depressions are large ($> 10^4$ $m^3$), the soil feedback imposes the strongest negative effect on stabilizing depression size, followed by the biomass feedback. The difference in ET rate between depression area and upland matrix is also a negative feedback, but of very weak strength (Figure 4(A)). Under the realistic scenario, the equilibrium depression volume is ~$6.4 \times 10^4$ $m^3$. With biomass feedback turned off (i.e. eliminating the negative effect of hydrology on biomass accrual in depressions), the equilibrium size is ~20% greater. When the soil cover feedback is turned off (i.e. $CO_2$ retention does not decline with thickness of soil cover on limestone bedrock), the depression volume at equilibrium state increases by ~300%. Lastly, turning off ET feedback only increases the volume at steady state about ~6%.

Expansion in volume of depressions leads to decline in the weathering rate of upland matrix (Figure 4(C)). The strength of this distal negative feedback is influenced by catchment area, with a stronger negative effect when the catchment area is smaller (Figure 4(B)). The stable steady state of basin depth is reached when the weathering rate of upland matrix equals that of depressions (Figure 4(C)). Such a steady state exists even though model runs did not reach steady state after 0.4 million years (the expansion in both radius and depths becomes extremely slow).

Throughout landscape development (over 0.4 million years modeled period), bedrock weathering is mostly reaction-limited, i.e. supply of $CO_2$ < export capacity of $Ca^{2+}$. Given the assumed initial conditions, only during the period between 13 kyr and 16 kyr (corresponding to the period of peak weathering rate in the course of landscape evolution) since landscape initiation is the weathering rate export limited (when export capacity is ~80% of the capacity needed to export available weathered $Ca^{2+}$; Figure S2). However, the absolute duration of export limitation is sensitive to the calcium concentration in the flow to groundwater and to surface flow set in the model. Slightly lower export concentrations than used in our simulations would result in transport limitation throughout the initial period of basin expansion, up to and potentially well beyond the current size of depressions. Regardless of the choice of concentrations, export of weathering products is largely reaction limited over the entire timespan required to reach landform equilibrium (Figure S2). The balance of reaction and transport processes is also sensitive to feedbacks. Turning off the biomass feedback, export limitation lasts between 8 kyr and 1.3 kyr after landscape initiation, during which reaction capacity is 210% of export capacity. With $CO_2$ feedback turned off, during half of the 0.2 million years modeled, landscape weathering is export limited, and the reaction capacity exceeds export capacity by 350% at maximum.

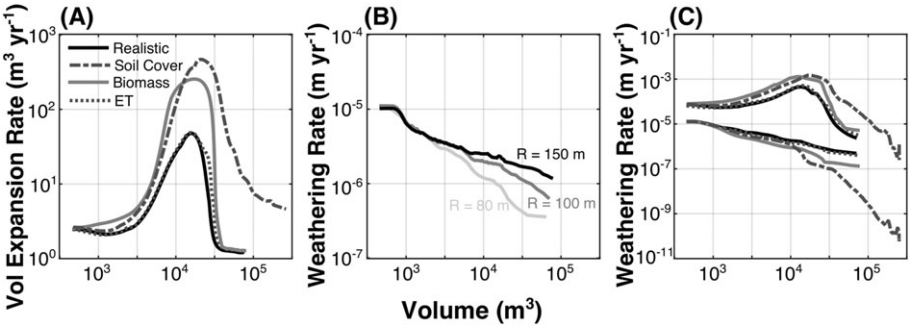


**Figure 4.** Ecohydrologic feedbacks and steady state of depressions. (A) The relative importance of three feedbacks (soil cover feedback, ET feedback, and biomass feedback) quantified by the volume expansion rate vs volume relationship. (B) The relationship between upland weathering rate vs volume relationship using three different catchment radiuses ($R$ = 80 m, 100 m, and 150 m). (C) Upland weathering rate (the lower four lines) and depression weathering rate (the upper four lines) as a function of volume in the four scenarios (as in (A)): when the value of these two rates are equal, stable steady state is reached (light gray solid dots). The solid black line in (A) and (B) represents the case when all three feedbacks are turned on in the model. Each model runs for 0.2 million years.

### Model analysis

Changing the precipitation regime, catchment size, and regional groundwater discharge rate do not preventing depressions from reaching equilibrium. However, they change the time required to reach equilibrium and the equilibrium size. Increase in annual precipitation or increase in catchment size can both increase the depression size at equilibrium (Figure 5).

We find that increasing the rate of groundwater discharge from 0.2 m $yr^{-1}$ to 0.6 m $yr^{-1}$ or decreasing the discharge to 0 both reduce the rate of depression volume expansion. However, the net effect of reducing discharge from 0.2 m $yr^{-1}$ to 0 is much greater than tripling the discharge rate (Figure 5).

## Discussion

In this study, we modeled multiple mechanisms that influence the development of cypress depressions in a low relief karst landscape in South Florida. We found strong evidence that a suite of local positive feedbacks favors relatively rapid expansion of depressions; however, we also found that expansion rates are insufficient to account for the current size (radius) of depressions in the patterned Big Cypress landscape, given the known time scale of their development. This suggests that depressions may have grown to their current size through coalescence rather than strictly by expansion. Consistent with the hypothesis that depressions inhibit weathering of near neighbors more strongly than distant ones, we found that the inhibitory effect of depressions on upland weathering rate decreased with catchment size (Figure 4(B)). The regular patterning of wetland depressions may arise from scale dependent feedbacks of weathering rate as groups of rapidly coalescing depressions compete for runoff. A model that more explicitly represents these spatial processes would increase our confidence in these inferences.

Our model indicates that the sizes and weathering rates in cypress depressions are not in equilibrium with upland weathering rates. The eventual equilibrium depth of depressions under conditions that prevail in Big Cypress is ~2–3 times their current depth. Of the potential negative feedbacks that might stabilize depression size, we found that the inhibitory effect of soil deepening on $CO_2$ transport, and the loss of vegetation due to impoundment contributed most strongly to reducing the future rate of wetland expansion. In contrast, growth of landscape ET with expansion of depressions had a relatively minor effect on the relationship between weathering rates and depression size. We suggest that the Big Cypress landscape is a useful laboratory for understanding ecomorphodynamic and ecohydrologic feedbacks. Extending this understanding and approach to different climatic and geologic settings may help better explain the evolution of biogeomorphic landscapes.

### Evolution of cypress depressions

Cypress depressions in South Florida represent a distinctive feature generated by ecohydrologic feedbacks between biology, hydrology, and morphological changes by chemical weathering of limestone bedrock. The self-organization of the landform has coincided with the history of regional climate. Triggered by the onset of a modern precipitation pattern in low-latitude regions, a major shift in vegetation pattern occurred in South Florida during the early Holocene (Watts and Hansen, 1994; Donders *et al.,* 2005). Pollen records show that around that time, *Pinus cf. elliottii* was gradually replaced by more inundation-tolerating *Taxodium* sp. in Big Cypress, which eventually became dominant (Donders *et al.,* 2005). The estimated age of the Big Cypress landscape (i.e. 7000–8000 years; Chamberlin *et al.,* 2018; Dong *et al.,* 2018) is slightly older than the arrival of cypress trees. This suggests that although most limestone weathering likely occurred during the cypress-dominated period when the climate was wet, the formation of depressions could have started before that, albeit at a very slow rate.

Ecohydrologic feedbacks not only control the rate but also the trajectory of landscape evolution. In our study, expansion of depressions at the early stage of landscape development is highly auto-catalytic (i.e. positive feedback; Figure 4(A)). In both absolute and relative terms, expansion of depressions accelerates radially and vertically for a period of approximately 10 000 years under conditions that prevail in Big Cypress. Vertical expansion decelerates rapidly after achieving a depth of ~3 m (Figure 3(E)), but radial expansion decelerates slowly over a much longer period (Figure 3(D)). The absolute rates in lateral and vertical expansion are of similar magnitude at a given depression volume during this initial expansion in the model. This symmetry of weathering would lead to spherical depressions, but existing Big Cypress depressions are orders of magnitude wider than deep. We thus infer that expansion of depression radius likely occurs through coalescence of neighboring small depressions in the early stage of landscape development. While our model did not explicitly simulate depression coalescence and we do not have direct evidence supporting this hypothesis, karst features developing via coalescences is a common phenomenon (Waele *et al.,* 2009). Moreover, without basin coalescence, the radius–depth ratio would imply that the mean weathering rate on the edge of a depression is about 25–45 times that in the center of depressions. In the present landscape, depression centers have longer hydroperiods, deeper

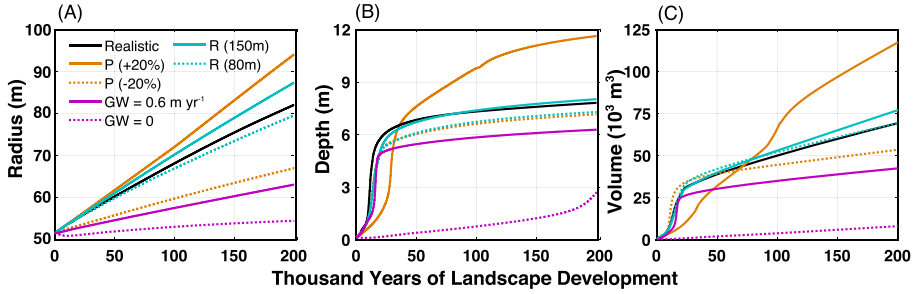


**Figure 5.** Changes of cypress depression radius (A), depth (B), and volume (C) over time under different scenarios: (1) precipitation (mean annual precipitation +20% or - 20% of current condition of 1337 mm $yr^{-1}$), (2) catchment size (change the catchment radius from 100 m to 150 m and 80 m), and (3) rate of regional groundwater discharge (increase the rate from 20 cm $yr^{-1}$ to 60 cm $yr^{-1}$and reduce to 0). Black solid line: current condition (realistic scenario). [Colour figure can be viewed at wileyonlinelibrary.com]

soils near the optimal depth for weathering, and higher biomass compared with the edge of depressions, all of which suggest that the opposite is more likely.

The overall positive feedback that drives initial basin expansion involves many more mechanisms than the classic karstification feedback between flow concentration and weathering rate (Sauro, 2012). These mechanisms are closely mediated by hydrological processes through their effect on vegetation growth and weathering. Increased capture of surface runoff by depressions improves hydrologic condition for plant growth, which enhances supply of $CO_2$. Extended periods of inundation also reduce atmospheric $CO_2$ loss, which increases the proportion of biogenic $CO_2$ retained for weathering (Dong *et al.,* 2018). Moreover, accelerated weathering and greater biomass contribute to sediment accumulation and soil development in depressions, facilitating further vegetation establishment – a positive feedback at relatively shallow soil depths (Figure 4(A)). Further expansion in volume however limits net $CO_2$ available for weathering at the bedrock surface by limiting biomass accrual (as a consequence of water deepening and extended inundation; i.e. a biomass feedback), and reducing $CO_2$ retention (as a consequence of soil thickening; i.e., a soil cover feedback). Eventually, volume expansion feeds back to reduce the rate of volume expansion – a negative feedback (Figure 4). Such self-limiting feedbacks with initial positive feedbacks have also been reported in other cases of karst biogeomorphic evolution, such as epikarst weathering and soil deepening by tree roots (Phillips, 2018). In Big Cypress, the soil cover feedback is stronger than the biomass feedback in stabilizing depression expansion, followed by ET feedback, which provides a very weak negative feedback (Figure 4). Originally, we hypothesized that as cypress depressions expand in volume, the landscape increases the fraction of water lost to ET, which reduces water loss via surface and groundwater drainage, and hence, lowers capacity to export weathering products. In part, the effectiveness of the volume expansion feedback is due to the loss of water from depressions via ET. However, the modest (20%) differences in ET between the uplands and depressions limit the strength of this direct ET feedback. Moreover, the weathering rate in Big Cypress may be reaction limited under current discharge–concentration relationships; hence, the ET feedback, while negative, is weak.

Model results suggest that the depressions in the Big Cypress landscape are far from equilibrium, and that depressions will continue to grow (albeit slowly) and eventually stabilize as large (~80 m radius), relatively deep (~ 7.5 m) depressions (Figure 3). We do not have direct measurements from the field of the weathering rate and direct assessment of changes of depression volume is not feasible at the time scale of a few years. However, dissolved $CO_2$ concentration can be used to infer weathering rate. Dissolved $CO_2$ concentration is about 3–4 times higher in the center of a depression (~6100 ppm) than that on the upland matrix (~1500 ppm), indicative of the much higher weathering capacity of depressions than uplands (data not published). Therefore, it is highly likely that current depressions in Big Cypress are still expanding in size.

As cypress depressions expand, their size eventually limits the growth and recruitment of cypress trees, as the water depth in the center of the depression is too deep for both processes. It is reasonable to predict that cypress 'domes' will become open water 'lakes' with cypress trees (or other riparian trees such as willows, observed in some domes on the current landscape) growing on the edge of the lake, as the landscape continues to evolve. In fact, in a few large cypress domes, the center has already converted to open water, with dead cypress tree logs, likely caused by large water depths and year-long inundation.

While the expansion of individual depressions to their steady state will not change the landscape spatial pattern (i.e. spatial arrangement of depressions), it will have significant ecological consequences. Continued expansion and deepening of cypress depression will alter the duration of inundation, the spatial distribution of water depth, and the connectivity among depressions, all of which will substantially modify the habitat for the large number of species (e.g. wading birds, reptile, fish, plant community) residing on this landscape. Many of these taxa are very sensitive to slight changes in water depth and/or hydro-period (Bancroft *et al.,* 2002; Sklar *et al.,* 2002).

Long before the system reaches its morphometric equilibrium, the Big Cypress landscape is likely to be inundated by ocean water. The elevation of Big Cypress National Preserve is only ~1–4 m above current sea level, and past and future variations in sea level are much greater at the time scale of a million years. Therefore, the ecological consequences of changes in depression may not be meaningful taking into consideration future changes in sea level. In addition, the model assumed a constant contemporary climate regime (precipitation and temperature) into the future 0.4 million years. Changes in precipitation and temperature would alter the rate of chemical weathering, hence, the rate of landscape evolution and the steady-state size of depressions (Figure 4). Interestingly, the transient exposure and inundation of coastal karst landforms may leave a signature of depression development in shallow seas. Regularly patterned limestone depressions have been found on the seafloor in other places around the world, e.g. Red Sea and Arabian Gulf (Purkis *et al.,* 2010). Those reticulated depressions are reported to form when sea level was lower and the sea floor was exposed, and the dissolution of the pattern initiated quickly at the onset of the Holocene wet phase (Purkis *et al.,* 2010). Big Cypress may also become one of these patterned limestone depressions under sea in the near future, with continued climate change.

## Feedbacks in biogeomorphic landscapes

Geomorphic and biological processes in a landscape have been largely conceptualized as independent, and reciprocal interactions between the two have been only recently acknowledged (Swanson *et al.,* 1988; Bendix and Hupp, 2000; Stallins, 2006; Murray *et al.,* 2008; Hupp *et al.,* 2016; Phillips, 2016b). It is increasingly recognized that for some systems, broad scale landscape topography arises from feedbacks between geomorphic and ecological processes, i.e. biogeomorphic feedbacks. The strength of biogeomorphic feedbacks in shaping landforms varies among systems, ranging from weak indirect impacts to strong direct impacts (e.g. landforms as extended phenotypes; Phillips, 2016b). At one extreme, landscape topography could be controlled directly by biological behaviors, coupled with geomorphic processes. For instance, evenly spaced termite mounds in semi-arid savanna result from interaction between territorial behavior of termites and scale-dependent feedbacks mediated by water use efficiency (Bonachela *et al.,* 2015; Pringle and Tarnita, 2017). More commonly, biogeomorphic feedbacks manifest in the form of vegetation interacting with sediment transport, erosion, and weathering (Baas, 2002; Gurnell *et al.,* 2005; Murray *et al.,* 2008). For example, in fluvial landscapes, the emergence of vascular plants during the late Silurian and Devonian periods instigated a shift from rivers with wide sand-beds to channelized meandering rivers with muddy floodplains, as a result of roots stabilizing the banks of rivers and streams (Murray and Paola, 2003; Tal *et al.,* 2004; Gibling and Davis, 2012). Recently, Schwarz *et al.* (2018) showed that plant life-history traits

can influence the evolution of coastal wetland landscapes, with fast colonizers facilitating the stabilization of existing channels and consolidating the current landform, while slow colonizers favor the formation of new channels and further landscape self-organization.

Here, we provide a case study of vegetation via biogeomorphic feedbacks creating limestone depressions across a flat landscape by accelerating chemical weathering of bedrock – i.e. karst biogeomorphology. A significant role for biota – particularly the role of biogenic $CO_2$ in accelerating limestone weathering – has long been recognized in karst landforms (Viles, 1984; Jennings, 1985; Ford and Williams, 2007). In Big Cypress, $CO_2$ subsidies from root and soil respiration accelerated weathering rate by ~20-fold (Dong *et al.,* 2018) – that is, without the acidity provided by biological respiration, the system would have looked like a limestone pavement with pits ~10 cm deep.

The strength of the feedbacks we identify is likely to vary among karst landforms in different regions, resulting in a wide range of variations in karst morphology. In Big Cypress, reduction of respirational $CO_2$ and its retention imposes a strong negative effect on the size of depressions (Figure 4(A)). When weathering rate in depressions equals that in the upland, the depth of depressions reaches a stable steady state (Figure 4(C)). The equilibrium size is therefore determined by the rate at which the weathering rate declines with increase in volume and the rate of upland weathering. Many factors could therefore shift the location of equilibrium by affecting one or both of these two factors. In the coastal Yucatan (Mexico) sinkholes, the land surface sits higher above sea level, so that vertical drainage is less restricted than in Big Cypress. Moreover, a high concentration of $H_2S$ is observed in the water of cenotes as a consequence of the reduction of the accumulated organic matter (Stoessell *et al.,* 1993). As a consequence, neither the volume feedback nor the negative $CO_2$ feedback is effective and sinkholes in Yucatan reach $>$ 100 m depth (Schmitter-Soto *et al.,* 2002). Precipitation also plays a role in constraining landform (Figure 5). With everything else being equal, higher precipitation moves equilibrium size to a larger value by slowing down the rate of decline of weathering rate in depressions (Figure 4(C); Figure 5). This may partly explain why labyrinth and associated tower karst are more common in humid tropical than in dry regions (Brook and Ford, 1978).

The local positive feedback between volume and the expansion of volume in the initial stage of rapid depression expansions generates distal negative feedbacks inhibiting the weathering of the associated catchment (Figure 4) and the capture of water by neighboring depressions (i.e. competition among depressions for water). The distal negative feedbacks become stronger as depressions expand and the area of associated catchment decreases (Figure 4(B)). Such scale-dependent feedbacks – local positive and long-distance negative feedback – likely contributed to the regular patterning of depressions in Big Cypress (Watts *et al.,* 2014), as it has in many other places (Rietkerk *et al.,* 2004). Interestingly, while the spatial arrangement of cypress depressions at the landscape scale are already strikingly regular (Watts *et al.,* 2014), indicating the completion of landscape self-organization, its components – the individual depressions – are not in equilibrium yet, according to our model (Figure 2). This suggests a decoupling of landscape-scale self-organization and the self-organizing of its constituent agents. Such independence of the dynamics at the landscape scale and at the constituent agent scale is also observed in other self-organized landscapes. For example, fairy circles (nearly circular barren patches within a sparse matrix of small short-lived grass species) in Namibia have a life history of birth, maturation, and death (become revegetated) over about 41-yr cycle, while at the landscape scale, the spatial arrangement of these bare patches remains regularly-spaced (Tschinkel, 2012). Our ability to link landscape and patch equilibria is admittedly limited to date, because our model simulated the dynamics of one depression and the catchment in which it is imbedded. A landscape-scale model that explicitly captures the interactions among multiple depressions and catchments is needed as a formal test of mechanisms giving rise to spatial overdispersion of cypress depressions across the landscape, and its relation to the dynamics of individual basins.

## Conclusion

Multiple ecohydrologic feedbacks mediate the expansion of cypress depression on a limestone landscape in South Florida. These feedbacks were initially positive with expansion of depressions resulting in accelerating volume expansion. However, as depressions become larger, the percentage of $CO_2$ reaching bedrock for weathering decreased rapidly, deep water in depressions become unfavorable for riparian tree growth, and the capacity to export weathering products declined. These factors ultimately stabilize the size of depressions. Model results suggest that cypress depressions are not yet in steady state and would continue to expand for a long time (at least 0.2 million years, if environmental conditions were to remain constant). However, at such a large time scale, any ecological consequences caused by changes in depressions will likely be moot given the much greater impacts of climate changes and sea-level rise.

*Acknowledgements*—This project is funded by National Science Foundation award DEB#1354783 (PIs: MJ Cohen, JB Heffernan, DL McLaughlin, JB Martin and A.B. Murray). This work used the high-throughput computation cluster at Duke Research Computing from Duke University. Site accesses were enabled by the US National Park Service under permit #BICY-2016-SCI-0008. We thank Stuart G. Fisher and two anonymous reviewers for their comments and edits, which significantly improved the paper.

## References

Acharya S, Kaplan DA, Casey S, Cohen MJ, Jawitz JW. 2015. Coupled local facilitation and global hydrologic inhibition drive landscape geometry in a patterned peatland. *Hydrology and Earth System Sciences* **19**: 2133–2144.

Baas ACW. 2002. Chaos, fractals and self-organization in coastal geomorphology: simulating dune landscapes in vegetated environments. *Geomorphology* **48**: 309–328.

Bancroft GT, Gawlik DE, Rutchey K. 2002. Distribution of wading birds relative to vegetation and water depths in the northern everglades of Florida, USA. *The International Journal of Waterbird Biology* **25**: 265–277.

Bendix J, Hupp CR. 2000. Hydrological and geomorphic impacts on riparian plant communities. *Hydrological Processes* **1085**: 2977–2990.

Berner RA. 1992. Weathering, plants, and the long-term carbon cycle. *Geochimica Ct Cosmochimica Acta* **56**: 3225–3231.

Bolster CH, Saiers JE. 2002. Development and evaluation of a mathematical model for surface-water-flow within the Shark River Slough of the Florida Everglades. *Journal of Hydrology* **259**: 221–235.

Bonachela JA, Pringle RM, Sheffer E, Coverdale TC, Guyton JA, Caylor KK, Levin SA, Tarnita CE. 2015. Termite mounds can increase the robustness of dryland ecosystems to climatic change. *Science* **347**: 651–655.

Brook GA, Ford DC. 1978. The origin of labyrinth and tower karst and the climatic conditions necessary for their development. *Nature* **275**: 493–496.

Chamberlin CA, Bianchi TS, Brown AL, Cohen MJ, Dong X, Flint MK, Martin JB, McLaughlin DL, Murray AB, Pain A, Quintero CJ. 2018.

Mass balance implies holocene development of a low-relief karst patterned landscape. *Chemical Geology*. https://doi.org/10.1016/J.CHEMGEO.2018.05.029.

Cohen MJ, Watts DL, Heffernan JB, Osborne TZ. 2011. Reciprocal biotic control on hydrology, nutrient gradients, and landform in the greater everglades. *Critical Reviews in Environmental Science and Technology* **41**: 395–429.

Corenblit D, Steiger J, Gurnell AM, Tabacchi E, Roques L, Pascal B. 2009. Control of sediment dynamics by vegetation as a key function driving biogeomorphic succession within fluvial corridors. *Earth Surface Processes and Landforms* **1810**: 1790–1810.

D'Odorico P. 2000. A possible bistable evolution of soil thickness. *Journal of Geophysical Research-Solid Earth* **105**: 25927–25935.

Gibling MR, Davis NS. 2012. Palaeonoic landscapes shaped by plant evolution. *Nature Geoscience* **5**: 99–105.

Day FP, Megonigal JP. 1993. The Relationship between variable hydroperiod, production, allocation, and belowground organic turnover in forested wetlands. *Wetlands* **13**: 115–121.

Dietrich WE, Perron JT. 2006. The search for a topographic signature of life. *Nature* **439**: 411–418.

Donders TH, Wagner F, Dilcher DL, Visscher H. 2005. Mid- to late-holocene El Nino-southern oscillation dynamics reflected in the subtropical terrestrial realm. *Proceedings of the National Academy of Sciences of the United States of America* **102**: 10904–10908.

Dong X, Cohen MJ, Martin JB, McLaughlin DL, Murray AB, Ward ND, Flint MK, Heffernan JB. 2018. Ecohydrologic processes and soil thickness feedbacks control limestone-weathering rates in a karst landscape. *Chemical Geology*. https://doi.org/10.1016/j.chemgeo.2018.05.021.

Egli M, Mirabella A, Sartori G. 2008. The role of climate and vegetation in weathering and clay mineral formation in late quaternary soils of the Swiss and Italian Alps. *Geomorphology* **102**: 307–324.

Eppinga MB, de Ruiter PC, Wassen MJ, Rietkerk M. 2009. Nutrients and hydrology indicate the driving mechanisms of peatland surface patterning. *The American Naturalist* **173**: 803–818.

Fookes PG, Hawkins AB. 1988. Limestone weathering: its engineering significance and a proposed classification scheme. *Quarterly Journal of Engineering Geology and Hydrogeology* **21**: 7–31.

Ford DC, Williams P. 2007. *Karst Hydrogeology and Geomorphology*. John Wiley & Sons: Chichester.

Gurnell A, Tockner K, Edwards P, Petts G. 2005. Effects of deposited wood on biocomplexity of river corridors. *Frontiers in Ecology and the Environment* **3**: 377–382.

Harms WR, Schreuder HT, Hook DD, Brown CL, Shropshire FW. 1980. The effects of flooding on the swamp forest in Lake Ocklawaha, Florida. *Ecology* **61**: 1412–1421.

Heffernan JB. 2008. Wetlands as an alternative stable state in desert streams. *Ecology* **89**: 1261–1271.

Heffernan JB, Watts DL, Cohen MJ. 2013. Discharge competence and pattern formation in peatlands: a meta-ecosystem model of the everglades ridge-slough landscape. *PLoS ONE* **8**: e64174.

Homoya MA, Hedge CL. 1982. The upland sinkhole swamps and ponds of Harrison County, Indiana. *Indiana Academy of Science* **92**: 383–388.

Hupp CR, Dufour S, Bornette G. 2016. Vegetation as a tool in the interpretation of fluvial geomorphic processes and landforms in humid temperate areas. In *Tools in Fluvial Geomorphology*, Kondolf GM, Piegay H (eds). John Wiley and Sons: Chichester.

Istanbulluoglu E, Bras RL. 2005. Vegetation-modulated landscape evolution: effects of vegetation on landscape processes, drainage density, and topography. *Journal of Geophysical Research* **110**: 1–19.

Jennings JN. 1985. *Karst Geomorphology*. Blackwell: Oxford.

Kadlec RH. 1990. Overland flow in wetlands: vegetation resistance. *Journal of Hydraulic Engineering* **116**: 691–706.

Kadlec RH, Knight RL. 1996. *Treatment Wetlands*. Lewis: Boca Raton, FL.

Kirwan ML, Guntenspergen GR. 2010. Influence of tidal range on the stability of coastal marshland. *Journal of Geophysical Research: Earth Surface* **115**: F02009. https://doi.org/10.1029/2009JF001400.

Laio F, Tamea S, Ridolfi L, D'Odorico P, Rodriguez-Iturbe I. 2009. Ecohydrology of groundwater-dependent ecosystems: 1. Stochastic water table dynamics. *Water Resource Research* **45**: 1–13.

Larsen LG, Harvey JW. 2010. How vegetation and sediment transport feedbacks drive landscape change in the everglades and wetland worldwide. *The American Naturalist* **176**: E66–E79.

Maramathas AJ, Boudouvis AG. 2006. Manifestation and measurement of the fractal characteristics of karst hydrogeological formations. *Water Resources* **29**: 112–116.

Martin Y, Church M. 1997. Diffusion in landscape development models: on the nature of basic transport relations. *Earth Surface Processes and Landforms: The Journal of The British Geomorphological Group* **22**: 273–279.

McLaughlin DL, Kaplan DA, Cohen MJ. 2014. A significantly nexus: geographically isolated wetlands influence landscape hydrology. *Water Resources Research* **50**: 5329–5333.

Megonigal JP, Day FP. 1992. Effects of flooding on root and shoot production of bald cypress in large experimental enclosures. *Ecology* **73**: 1182-1193.

Mitsch WJ, Ewel KC. 1979. Comparative biomass and growth of cypress in Florida wetlands. *American Midland Naturalist* **101**: 417–426.

Murray AB, Knaapen MAF, Tal M, Kirwan ML. 2008. Biomorphodynamics: physical-biological feedbacks that shape landscapes. *Water Resource Research* **44**: 1–18.

Murray AB, Paola C. 2003. Modeling the effect of vegetation on channel pattern in bedload rivers. *Earth Surface Processes and Landforms* **28**: 131–143.

Phillips JD. 2016a. Landforms as extended composite phenotypes. *Earth Surface Processes and Landforms* **26**: 16–26.

Phillips JD. 2016b. Biogeomorphology and contingent ecosystem engineering in karst landscapes. *Progress in Physical Geography* **40**: 503–526.

Phillips JD. 2018. Self-limited biogeomorphic ecosystem engineering in epikarst soils. *Physical Geography* **39**: 304–328.

Pringle RM, Tarnita CE. 2017. Spatial self-organization of ecosystems: integrating multiple mechanisms of regular-pattern formation. *Annual Review of Entomology* **62**: 359–377.

Purkis SJ, Rowlands GP, Riegl BM, Renaud PG. 2010. The paradox of tropical karst morphology in the coral Reefs of the arid middle east. *Geology* **3**: 227–230.

Reddy KR, Delaune RD, Debusk WF, Koch MS. 1993. Long-term nutrient accumulation rates in the everglades. *Soil Science Society of America Journal* **57**: 1147–1155.

Rietkerk M, Dekker SC, de Ruiter PC, Koppel J. 2004. Self-organized patchiness and catastrophic shifts in ecosystems. *Science* **305**: 1926–1929.

Rietkerk M, van de Koppel J. 2008. Regular pattern formation in real ecosystems. *Trends in Ecology and Evolution* **23**: 169–175.

Rodriguez-Iturbe I, Porporato A, Ridolfi L, Isham V, Cox DR. 1999. Probabilistic modelling of water balance at a point: the role of climate, soil and vegetation. *Proceedings of the Royal Society of London A: Mathematical, Physical and Engineering Sciences* **455**: 3789–3805.

Roering JJ, Kirchner JW, Dietrich WE. 1999. Evidence for nonlinear, diffusive sediment transport on hillslopes and implications for landscape morphology oreo. *Water Resource Research* **35**: 853–870.

Sauro U. 2012. Closed depressions in karst areas. In *Encyclopedia of Caves*, White WB, Culver DC (eds). Academic Press: Cambridge.

Schenk HJ, Jackson RB. 2002. The global biogeography of roots. *Ecological Monographs* **72**: 311–328.

Schmitter-Soto JJ, Comín FA, Escobar-Briones E, Herrera-Silveira J, Alcocer J, Suárez-Morales E, Elías-Gutiérrez M, Díaz-Arce V, Marín LE, Steinich B. 2002. Hydrogeochemical and biological characteristics of Cenotes in the Yucatan peninsula (SE Mexico). *Hydrobiologia* **467**: 215–228.

Schwarz C, Gourgue O, van Belzen J, Zhu Z, Bouma TJ, van de Koppel J, Ruessink G, Claude N, Temmerman S. 2018. Self-organization of a biogeomorphic landscape controlled by plant-history traits. *Nature Geoscience* **11**: 672–677.

Shoemaker B, Lopez DC, Duever MJ. 2011. Evapotranspiration over spatially extensive plant communities in the big cypress national preserve, southern Florida, 2007–2010. US Geological Survey Scientific Investigations Report, 2011: 5212.

Sklar F, McVoy C, VanZee R, Gawlik DE, Tarboton K, Rudnick D, Miao S, Armentano T. 2002. The effects of altered hydrology on the ecology of the everglades. In *The Everglades, Florida Bay, and Coral Reefs of the Florida Keys: an Ecosystem Sourcebook*. CRC Press: Boca Raton, FL.

Snyder JR. 1991. Fire regimes in subtropical south Florida. *Proceedings Tall Timbers Fire Ecology Conference* **17**: 303–319.

Stallins JA. 2006. Geomorphology and ecology: unifying themes for complex systems in biogeomorphology. *Geomorphology* **77**: 207–216.
Stoessell RK, Moore YH, Coke J. 1993. The occurrence and effect of sulfate reduction and sulfide oxidation on coastal limestone dissolution in Yucatan cenotes. *Ground Water* **31**: 566–575.
Strudley MW, Murray AB, Haff PK. 2006. Emergence of Pediments, Tors, and Piedmont junctions from a bedrock weathering-regolith thickness feedback. *Geology* **34**: 805–808.
Swanson FJ, Kratz TK, Caine N, Woodmansee RG. 1988. Landform effects on ecosystem patterns and processes. *BioScience* **38**: 92–98.
Tal M, Gran K, Murray AB, Paolo C, Hicks DM. 2004. Riparian vegetation as a primary control on channel characteristics in noncohesive sediments. In *Riparian Vegetation and Fluvial Geomorphology*, Sean JB, Simon A (eds), Vol. **8**, Water Science and Application. American Geophysical Union; 43–58.
Tarnita CE, Bonachela JA, Sheffer E, Guyton JA, Coverdale TC, Long RA, Pringle RM. 2017. A theoretical foundation for multi-scale regular vegetation patterns. *Nature* **541**: 398–401.
Tihansky AB. 1999. Sinkholes, wetland-central Florida. *Land Subsidence in the United States: US Geological Survey Circular* **1182**: 121–140.
Toy TJ, Foster GR, Renard KG. 2002. *Soil Erosion: Processes, Prediction, Measurement, and Control*. Wiley: New York.
Tschinkel WR. 2012. The life cycle and life span of Namibian fairy circles. *PLoS ONE* **7**: e38–e56.
Van Rees KCJ, Comerford NB. 1986. Vertical root distribution and strontium uptake of a slash pine stand on a Florida spodosol. *Soil Science Society of America Journal* **50**: 1042–1046.
Viles HA. 1984. Biokarst: review and prospect. *Progress in Physical Geography* **8**: 523–542.
Waele JD, Mucedda M, Montanaro L. 2009. Geomorphology morphology and origin of coastal karst landforms in Miocene and Quaternary carbonate rocks along the central-western coast of Sardinia (Italy). *Geomorphology* **106**: 26–34.
Watts AC. 2013. Forest ecology and management organic soil combustion in cypress swamps: moisture effects and landscape implications for carbon release. *Forest Ecology and Management* **294**: 178–187.
Watts AC, Kobziar LN, Snyder JR. 2012. Fire reinforces structure of pond cypress (*Taxodium Distichum* Var. Imbricarium) domes in a wetland landscape. *Wetlands* **32**: 439–448.
Watts AC, Watts DL, Cohen MJ, Heffernan JB, Mclaughlin DL, Martin JB, Kaplan DA, Osborne TZ, Kobziar LN. 2014. Evidence of biogeomorphic patterning in a low-relief karst landscape. *Earth Surface Processes and Landforms* **39**: 2027–2037.
Watts WA, Hansen BCS. 1994. Pre-holocene and holocene pollen records of vegetation history from the Florida peninsular and their climatic implications. *Palaeogeography Palaeoclimatology Palaeoecology* **109**: 163–176.

## Appendix A. Estimating Soil Respiration

Soil respiration is calculated using values from the literature and field data from Big Cypress when available. We first construct an empirical relationship between cypress tree height ($H$ in m) and thickness of soil cover ($z_s$ in m):

$$H_{tr} = \frac{H_{max}}{1 + e^{-b(z_s - a)}} \tag{A1}$$

which is the same as Equation (11) in the main text, with $H_{max}$ = 30 m, $b$ = 2, $a$ = 1.3. Cypress tree height is then correlated to tree diameter at breast height (DBH in cm) by DBH = 1.4754$H$ + 1.1629 ($R^2$ = 0.64). The relationship between DBH and aboveground dry mass ($bm$ in kg) is obtained from Mitsch and Ewel (1979) specific for cypress trees: $bm = e^{-2.2094+2.3867\ln(\mathrm{DBH})}$. According to Mitsch and Ewel (1979), the ratio of root dry biomass and aboveground biomass is 32–43% for cypress trees in Florida. Using this array of relationships, we can infer the root biomass from soil thickness at the location of the cypress tree.

Root biomass is further used to infer soil respiration. We assume a ratio of 1:15 for the fine root biomass (root diameter < 2 mm) and coarse root biomass (Ryan *et al.,* 1996). For fine roots, we use a respiration rate of $r_F = 1\times10^{-9}$ mol $CO_2$ $g^{-1}$ fine root $s^{-1}$ and assume that the respiration rate by coarse roots $r_C$ is 2% of that (Ryan *et al.,* 1996; Bouma *et al.,* 1997; Clinton and Vose, 1999). The average distance between two cypress trees in Big Cypress is about 2.29 m, i.e. 0.191 trees per $m^2$. Meanwhile, we assume that $CO_2$ production from organic decomposition is about the same as that by root respiration. Integrating all the information, soil $CO_2$ production rate, $P_{CO2}$ (g C $m^{-2}$ $yr^{-1}$) can be estimated directly given soil thickness. For example, for 1.5 m soil thickness, $CO_2$ production is 784 g C $m^{-2}$ $yr^{-1}$, for 1 m soil it is 368 g C $m^{-2}$ $yr^{-1}$, and for 0.5 m soil, it is 120 g C $m^{-2}$ $yr^{-1}$. These rates fall within the range of measured $CO_2$ production rates in the literature (Raich and Schlesinger, 1992).

## Appendix References

Bouma TJ, Nielsen KL, Eissenstat DM, Lynch JP. 1997. Estimating respiration of roots in soil: interactions with soil $CO_2$, soil temperature and soil water content. *Plant and Soil* **195**: 221–232.
Clinton BD, Vose JM. 1999. Fine root respiration in mature eastern white pine (*Pinus strobus*) in situ: the importance of $CO_2$ in controlled environments. *Tree Physiology* **19**: 475–479.
Mitsch WJ, Ewel KC. 1979. Comparative biomass and growth of cypress in Florida wetlands. *American Midland Naturalist* **101**: 417–426.
Raich JW, Schlesinger WH. 1992. The global carbon dioxide flux in soil respiration and its relationship to vegetation and climate. *Tellus B* **44**: 81–99.
Ryan MG, Hubbard RM, Pongracic S, Raison RJ, McMurtrie RE. 1996. Foliage, fine-root, woody-tissue and stand respiration in *Pinus radiata* in relation to nitrogen status. *Tree Physiology* **16**: 333–343.

## Supporting Information

Additional supporting information may be found online in the Supporting Information section at the end of the article.

**Table S1.** Description of variables used in the model and their values.

**Figure S1**. $CO_2$ retention as a function soil thickness on bedrock in two different hydrological states from the limestone weathering model by Dong et al. (*in press*) parameterized for conditions in Big Cypress National Preserve, South Florida. The two hydrologic states are: (1) inundated soil: when soil profile is completely inundated by surface flow across a whole year; (2) exposed soil: the initial condition of soils is completely saturated soil, but without surface flow cover. Soil moisture declines over time. '+' are model outputs under these two hydrologic states. Lines represent the best fit exponential decay curves. For inundated soil, it is $y = \frac{1.05}{e^{1.5\times\left(\frac{x}{100}+0.7\right)}}$; and for exposed soil, the best fit is $y = 0.88e^{2.6\times\left(\frac{x}{100}+0.7\right)}$.

**Figure S2.** Model sensitivity to the slope of the concentration of calcium in flows exporting via surface drainage and via groundwater drainage. During the evolution of a cypress depression, we assume a linear relationship between calcium concentrations and the volume of biomass in the system. In the initial condition, biomass is 0 and calcium concentration in exporting flows is in equilibrium with atmospheric $CO_2$ pressure (calcium in flow to surface water from depressions and to groundwater is 18.2 mg $L^{-1}$); and with present-day biomass, calcium concentration in surface flow moving out of a depression is 56 mg $L^{-1}$ and in groundwater is 158 mg $L^{-1}$. Another three

different combinations of surface water and ground water $Ca^{2+}$ concentrations were chosen (lines in gradient from black to light-gray: 56 and 158 mg $L^{-1}$, 38 and 107 mg $L^{-1}$, 34 and 96 mg $L^{-1}$, and 25 and 70 mg $L^{-1}$.) to construct the linear relationship to analyze the sensitivity.

**Figure S3.** Schematic illustration of weathering (blue arrow) in the upland matrix (A), which expands the area of the upland and reduces the volume of the depression, and weathering in the depressional area (B), which expands the area/volume of the depression and reduces the area of the upland. Dotted lines indicate the position of bedrock before weathering. After weathering, the bedrock surface is lowered to the position indicated by solid lines.